Study of Microwave Backscattering From Two-Dimensional Nonlinear Surfaces of Finite-Depth Seas

Ding Nie, Min Zhang, Chao Wang, and Hong-Cheng Yin

Abstract—**This paper presents a study of the microwave backscattering from 2-D time-evolving nonlinear surfaces of a sea with finite depth by using the second-order small-slope approximation. According to the shallow-water dispersion relation, the revised nonlinear hydrodynamic choppy wave model in connection with an experiment-verified sea spectrum for finite-depth water is employed to construct the wave profiles in the finite-depth sea. The numerical results show that the discrepancy between the choppy surfaces of the infinite-depth sea and their finite-depth counterparts for monostatic normalized radar cross section is much smaller than that between the linear surfaces and the nonlinear choppy surfaces. Furthermore, the comparison of the Doppler spectra of the backscattered echoes from the linear and nonlinear choppy sea surfaces shows that the nonlinear hydrodynamic features significantly impact the Doppler spectrum. In particular, the Doppler spectrum for nonlinear finite-depth sea presents much higher second-order peaks and increased spectral amplitudes in the frequency range around the Doppler peak frequency, which reiterates the importance of the role that the nonlinear hydrodynamic effect of waves played in the interpretation of backscattering from finite-depth nearshore seas from the qualitative point of view.**

Index Terms—**Doppler spectrum, finite-depth sea, microwave scattering, nonlinear sea surface, second-order small-slope approximation (SSA) (SSA-II).**

I. Introduction

The study of microwave scattering from oceanic surfaces has received great attention for its myriad applications in areas such as oceanic surveillance, target detection, and remote sensing in marine environment [1]–[6]. The appropriate description of the sea wave structure is prerequisite to investigate scattering from sea surfaces. The linear surface model remains in common use, which is a linear superposition of gravity harmonic waves with Gaussian random phases. However, in some complicated circumstance that the hydrodynamic nonlinearities of the sea waves should be considered, such as scattering analysis and Doppler spectrum interpretation for shallow sea, the simplest linear model seems incompetent.

Nonlinear hydrodynamics links the motion of waves with different scales, which lead to transformation of the wave shape. Based on this, some nonlinear models came into being and had been widely used. Rino *et al.* [7] comparatively studied the backscattering and the Doppler spectra from time-varying linear and nonlinear Creamer [8] sea surfaces. Toporkov and Brown [9], [10] made a comprehensive study of the Creamer nonlinear surface scattering characteristics. For other nonlinear sea-surface models such as the West model [11], Johnson *et al.* [12] and Hayslip *et al.* [13] carried out related research studies. Recently, Soriano *et al.* [14] have extended the Doppler spectral analysis to the 2-D nonlinear surfaces (3-D microwave scattering issues) from 1-D ones. Nouguier *et al.* [15] resorted to the so-called nonlinear “choppy wave model” (CWM) [16] probing the impact of nonlinear-wave profiles in scattering from sea surfaces. They [17], [18] also combined the CWM with the weighted curvature approximation (WCA) and derived related statistical expression to simulate ocean Doppler features at microwave frequencies. Thus, compared with the Creamer model and West model, the CWM has proven to enjoy some desirable properties such as analytical simplicity and numerical efficiency. Most of these studies are limited to infinite-depth sea, however.

In recent decades, Bitner [19] studied the nonlinear effects of shallow-water wind waves and drew the conclusion that the shallow-water wind waves can be treated like a quasi-normal random process, and the nonlinear effects may slightly decrease the mean wave height. Barrick and Lipa [20], [21] presented details of the analytical techniques for the modeling and inversion of second-order high-frequency (HF) radar Doppler spectra of sea echo, and they stressed that the energy in the second-order spectrum increases as the water depth decreases and the hydrodynamic contribution is more important when sea waves move into shallow water. Holden and Wyatt [22] discussed modifications necessary to account for the effects of shallow water in the simulation and inversion of radar Doppler spectra. Moreover, the related research on fluid mechanics [23] found that the energy transportation in shallow water is more efficient than that in deep water and the nonlinear-wave–current interactions and wave–wave interactions occur more frequently, which mainly control the shape and evolution of the wind-wave spectrum. Therefore, to simulate the structure of the finite-depth shallow-sea waves, the corresponding finite-depth sea spectrum should be considered. In general, as a wave propagates from an

Manuscript received September 26, 2011; revised February 27, 2012; accepted March 24, 2012. Date of publication May 23, 2012; date of current version October 24, 2012. This work was supported in part by the Fundamental Research Funds for the Central Universities, by the National Natural Science Foundation of China under Grant 60871070, and by the Foundation of National Key Laboratory of Electromagnetic Environmental Research.

D. Nie and M. Zhang are with the School of Science, Xidian University, Xi’an 710071, China (e-mail: dnie2007@yahoo.com.cn; mzhang@mail.xidian.edu.cn).

C. Wang and H.-C. Yin are with the Science and Technology on Electromagnetic Scattering Laboratory, Beijing 100854, China (e-mail: wangc207@gmail.com; yinhc207@yahoo.com.cn).

Color versions of one or more of the figures in this paper are available online at http://ieeexplore.ieee.org.

Digital Object Identifier 10.1109/TGRS.2012.2194716

infinite-depth sea to a finite-depth region, water depth decreases and the wave slows down, although its frequency remains the same. As a result, it changes shape: Its crest becomes shorter and steepens, while its trough lengthens and flattens out. Thus, the nonlinear CWM is much appropriate for constructing this kind of surface profiles. In this paper, we revised the CWM to take the infinite-depth effect into account. Moreover, we just consider sea surfaces of constantly finite depth, and the extra effects of wave energy dissipation such as breaking are certainly not taken into account. Based on the preceding analysis, the revised CWM combining with the finite-depth sea spectrum is more suitable to accurately describe the profiles of a finite-depth sea.

The small-slope approximation (SSA) theory comprises a basic approximation of the theory (SSA-I) and second-order corrections to it (SSA-II), which has been widely applied to evaluate microwave scattering from sea surfaces [24], [25]. It is a competent candidate to bridge the gap between the Kirchhoff approximation (KA) and the small-perturbation method (SPM). Compared with the KA and SSA-I, the SSA-II is capable of predicting polarization sensitivity (both copolarization and cross-polarization) for Doppler spectra, which is indispensable for studying Doppler characteristics of sea surfaces. The more recent WCA [17], [18] is also a promising analytical model, whose scattering amplitude is a correction to SSA-I and based on a combination of SPM and KA kernels that are evaluated at local angles; thus, it is a local model that cannot predict correct cross-polarization in the plane of incidence. Based on the consideration of the continuity of the future work for evaluation of the cross-polarization, thus, the SSA-II is employed in this study.

This paper is organized as follows. In Section II, the revised nonlinear CWM combining with the experiment-verified finite-depth sea spectrum is used to simulate 2-D surfaces of finite-depth seas. Section III presents the SSA-II model for evaluating the microwave backscattering from finite-depth sea in detail. Comparison of numerical results of the monostatic normalized radar cross section (NRCS) and Doppler spectra for infinite-depth sea and finite-depth sea is presented and discussed in Section IV. Section V is devoted to the conclusions of this paper.

II. Nonlinear Hydrodynamic Model for Finite-Depth Seas

A. Wind-Wave Spectrum in Finite-Depth Seawater

The simulations of deep sea mostly take the wind and the gravity as the kernel, which determine the propagation speed and the shape of the waves. The effect of water depth is usually neglected in the process of modeling deep water. When the waves propagate into shallow-sea region, however, it is essential that the water depth and seabed topography will change the shape and the statistical characteristics of the sea surface. Thus, compared with deep-sea spectrum, the shallow-sea spectrum will undergo a transformation accordingly. For most of available deep-sea spectra, such as Pierson–Moskowitz spectrum and Joint North Sea Wave Project (JONSWAP) spectrum, their HF flank can be described by a frequency dependence f^{-m}, with m being measured by a large number of experiments as lying between four and five, whereas for its counterpart of the shallow-sea spectrum, Kitaigordskii *et al.* [26] and Thornton [27] have reported that the depth of water becomes a relevant parameter and the index m is proposed to be less than four after it was measured by a series of shallow-water wave measurements. The TMA [TEXEL–Marine Remote Sensing Experiment at the North Sea (MARSEN)-Atlantic Ocean Remote Sensing Land-Ocean Experiment (ARSLOE)] spectrum for finite-depth waves is used in this paper, which was proposed in a relatively comprehensive study of finite-depth wave spectra of Bouws *et al.* [28]. This study comprised measurements made at coastal sites during three field experiments (TEXEL in the Dutch North Sea, MARSEN in the German Bight, and ARSLOE in the U.S. east coast). The spectrum of actively growing wind waves in finite-depth sea can be analytically expressed as

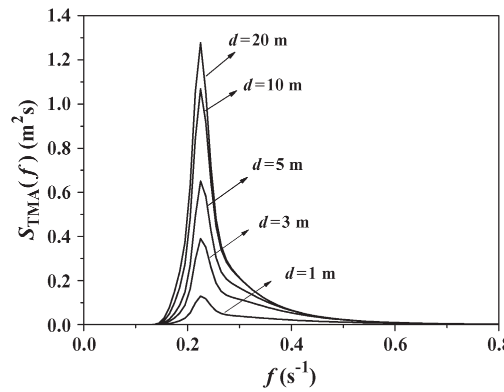

Fig. 1. TMA sea spectra for different water depths d.

$$S_{\mathrm{TMA}}(f) = S_J(f)\Phi(d) \tag{1}$$

with

$$S_J(f) = \frac{\alpha g^2}{(2\pi)^4 f^5} \exp\left[-1.25\left(\frac{f_m}{f}\right)^4\right] \gamma^{\exp\left[\frac{-(f-f_m)^2}{2\sigma^2 f_m^2}\right]} \tag{2}$$

$$\Phi(d) = \frac{[k(f,d)]^{-3}\,\frac{\partial k(f,d)}{\partial f}}{[k(f,\infty)]^{-3}\,\frac{\partial k(f,\infty)}{\partial f}} = \frac{\tanh^3(kd)}{\tanh(kd) + kd - kd\tanh^2(kd)} \tag{3}$$

where $S_J(f)$ is the JONSWAP spectrum, f is the frequency of the sea wave, f_m is the spectrum peak frequency, and g is the acceleration of gravity. The Phillips parameter α changes as the wind speed u at a height of 10 m. The factors γ and σ exhibit no trend as functions of u. The exact value of the aforementioned parameters can be referred to [29]. $k(f,d)$ is the wavenumber of the sea wave, which is related to f and water depth d according to the shallow-water gravity–capillarity dispersion relation as $f = \sqrt{gk(1 + k^2/k_m^2)\tanh(kd)}/2\pi$, where $k_m = 363.2$ rad/m is the wavenumber with minimum phase speed. The function $\Phi(d)$ is applied to describe the upper bound of the equilibrium range of the spectrum, meanwhile. When d is chosen to be infinite, the spectrum is just the JONSWAP spectrum for infinite-depth sea.

Fig. 1 just shows the influence of the water depth to the TMA spectrum. From Fig. 1, it is evident that the slope of the HF part of the spectrum is much more flat as the seawater depth decreases. Compared with deep-water sea spectrum, the TMA spectrum is more competent in the subsequent surface realizations of the finite-depth sea.

B. Sea-Surface Realizations

To study the time-evolving scattering characteristics of the sea surface correctly, the geometric property of the sea surface should be captured in detail. For the fully developed infinite-depth sea, the spectral method is applied to yield a linear superposition of harmonic waves whose amplitudes are independent normal-distributed random values times the square root of the sea-surface spatial spectrum. This is most efficiently accomplished directly in the Fourier domain. The Fourier amplitudes of a sea-surface elevation at time t can be expressed as

$$A(\mathbf{k},t) = \Upsilon(\mathbf{k})\sqrt{S(\mathbf{k},\varphi)\delta k_x \delta k_y}\exp(j\omega t) + \Upsilon(-\mathbf{k})^* \sqrt{S(\mathbf{k},\pi-\varphi)\delta k_x \delta k_y}\exp(-j\omega t) \quad (4)$$

where $\mathbf{k} = (k_x, k_y)$ is a 2-D vector with components of $k_x = n\delta k_x$ and$k_y = m\delta k_y$. n and m are the sampling numbers. The sampling intervals $\delta k_x = 2\pi/L_x$ and $\delta k_y = 2\pi/L_y$ are related to the lengths of the 2-D sea surface along x-axis direction L_x and y-axis direction L_y, respectively.$\Upsilon(\mathbf{k})$ is a complex Gaussian series with zero mean and unity standard deviation. Based on the gravity–capillarity dispersion relation, angular frequency $\omega = \sqrt{gk(1+k^2/k_m^2)}$ is for deep seawater, and $\omega = \sqrt{gk(1+k^2/k_m^2)\tanh(kd)}$ is for finite-depth seawater. $S(k,\varphi)$ is the 2-D deep-sea or shallow-sea spectrum taking the wind direction into account. Here, we assume that the direction along the positive x-axis direction coincides with the downwind direction. Thus, the sea-surface elevation h at position $\mathbf{r} = (x,y)$ and time t can be expressed as

$$h(\mathbf{r},t) = \sum_{\mathbf{k}} A(\mathbf{k},t)\exp(j\mathbf{k}\cdot\mathbf{r}). \quad (5)$$

Equation (5) can be efficiently accomplished by inverse fast Fourier transform, and the Hermitian form of (4) ensures that $h(\mathbf{r},t)$ is real.

The nonlinear hydrodynamic model CWM is based on a Lagrangian description of sea wave motion and can be constituted by horizontal displacement of Hilbert transform of an aforementioned linear surface. The displacement is written as

$$\mathbf{C}(\mathbf{r},t) = \sum_{\mathbf{k}} -j\frac{\mathbf{k}}{k}h(\mathbf{r},t)\exp(j\mathbf{k}\cdot\mathbf{r}). \quad (6)$$

When we focus on the finite-depth surface case, this displacement should be affected by the finite-depth factor. More recently, a stochastic Lagrange wave model that can describe surfaces of the finite-depth sea has gained increasing attention [30]–[32]. The original version of such a model can be found in the Miche model [33]. Inspired by this, we can rewrite (6) after taking the finite-depth factor into consideration

$$\mathbf{C}_f(\mathbf{r},t) = \sum_{\mathbf{k}} -j\frac{\mathbf{k}}{k}\frac{\cosh(kd)}{\sinh(kd)}h(\mathbf{r},t)\exp(j\mathbf{k}\cdot\mathbf{r}). \quad (7)$$

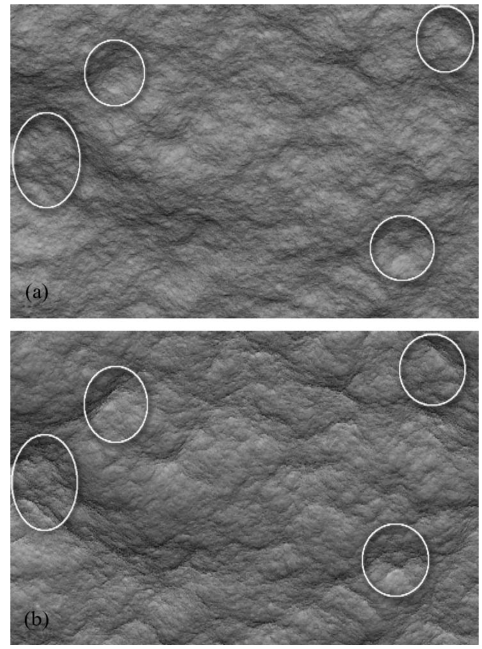

Fig. 2. Simulated (a) linear infinite-depth sea surface and (b) 5-m-deep nonlinear choppy sea surface. The wind speed is 6 m/s.

When the water depth d tends to infinite, then (7) reduces to (6). Using this vector field, the horizontal position of a grid point of the sea surface is now $\tilde{\mathbf{r}} = \mathbf{r} + \mathbf{C}_f(\mathbf{r},t)$, with elevation $\tilde{h}(\tilde{\mathbf{r}},t) = h(r,t)$ as before. Compared with the classical linear sea wave, this particular warping in the nonlinear model sharpens the wave peaks and broadens the wave valleys, which is a nonlinear hydrodynamic behavior that makes the sea surface generated more consistent with the real sea surface of the finite-depth sea.

Fig. 2 shows the comparison of the 2-D bird's-eye view of the linear infinite-depth sea and the nonlinear finite-depth choppy sea, the wind speed is 6 m/s, and the depth of the shallow sea is 5 m. From the comparison of the circles at the corresponding same position in Fig. 2(a) and (b), it is found that the crests of the finite-depth choppy sea are sharpened while those of the linear sea are smoother.

To clearly show the influences of nonlinear hydrodynamics and finite-depth factor on the geometric appearance of the surface, a comparison of 1-D sea-surface profiles is shown in Fig. 3. In Fig. 3(a), it is much easier to observe that, for the nonlinear choppy surface wave, their peaks become much steeper than that of the linear wave but their troughs flatten out. This consists of the conclusion drawn from Fig. 2. From the comparison in Fig. 3(b), it is found that the finite-depth factor also influences the profile shape. To a certain extent, as the water depth decreases, the wave crests steepen while wave troughs become much gentler. This property of the nonlinear hydrodynamic finite-depth wave model is more consistent with the actual shallow-sea waves.

III. SSA-II Model for Backscattering From 2-D Surfaces of Finite-Depth Seas

Consider a tapered plane wave illuminating upon a 2-D rectangle sea surface $L_x \times L_y$ to eliminate the edge effect caused

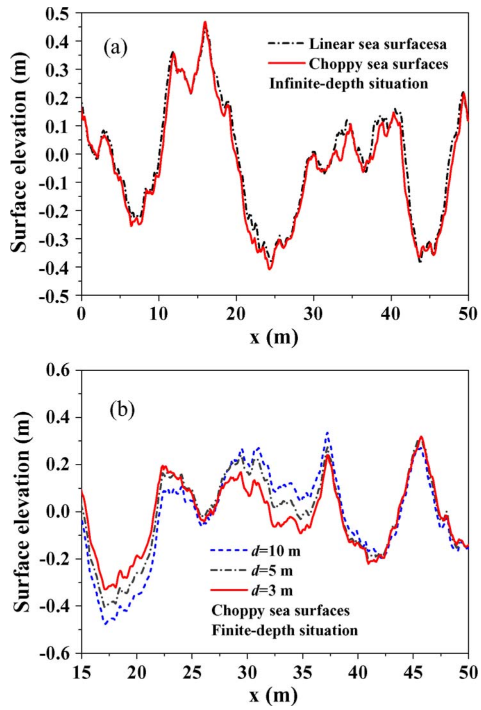

Fig. 3. Comparison of 1-D sea-surface profiles. (a) Linear surface and nonlinear choppy surface of infinite-depth sea. (b) Nonlinear choppy surfaces of finite-depth sea with different water depths. The wind speed is 6 m/s.

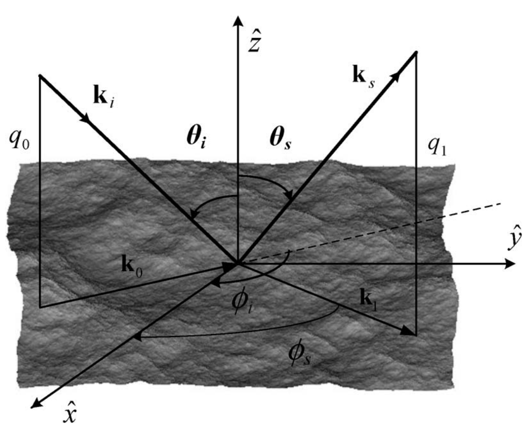

Fig. 4. Geometry of the sea-surface scattering problem.

by choosing limited size surface. The geometry of the scattering problem is shown in Fig. 4. θ_i and ϕ_i denote the incident angle and incident azimuth angle, respectively, while θ_s and ϕ_s represent the scattering angle and scattering azimuth angle, respectively. The incident wave vector $\mathbf{k}_i$ and scattering wave vector $\mathbf{k}_s$ can be decomposed into their horizontal components and vertical components, respectively (see Fig. 4)

$$\mathbf{k}_i = \mathbf{k}_0 - q_0\hat{\mathbf{z}} \quad \mathbf{k}_s = \mathbf{k}_1 + q_1\hat{\mathbf{z}} \tag{8}$$

where $k_0^2 + q_0^2 = k_1^2 + q_1^2 = k_i^2$; meanwhile, q and q_0 both should be larger than zero. The tapered incident field can be expressed as

$$\mathbf{E}_i(\mathbf{r}) = \mathbf{G}(\mathbf{r}, h)\exp(-j\mathbf{k}_i \cdot \mathbf{r}) \tag{9}$$

with the 2-D taper function $\mathbf{G}(\mathbf{r})$ detailedly defined in [34]. Thus, the scattering amplitude of the SSA-II model for linear sea is expressed as

$$\begin{aligned}\mathbf{S}(\mathbf{k}_i, \mathbf{k}_s; t) = &\frac{2\sqrt{q_0 q_1}}{(q_0+q_1)\sqrt{P}} \int \frac{d\mathbf{r}}{(2\pi)^2}\mathbf{G}(\mathbf{r}, h)\\ &\times \exp\left[-j(\mathbf{k}_1 - \mathbf{k}_0)\cdot\mathbf{r} + j(q_1+q_0)h(\mathbf{r}, t)\right]\\ &\times \Bigg(B(\mathbf{k}_1, \mathbf{k}_0) - \frac{j}{4}\int M(\mathbf{k}_1, \mathbf{k}_0; \boldsymbol{\xi})\mathbf{H}(\boldsymbol{\xi}, t)\\ &\times \exp(j\boldsymbol{\xi}\cdot\mathbf{r})d\boldsymbol{\xi}\Bigg)\end{aligned} \tag{10}$$

where

$$\mathbf{H}(\boldsymbol{\xi}, t) = \frac{1}{(2\pi)^2}\int h(\mathbf{r}, t)\exp(-j\boldsymbol{\xi}\cdot\mathbf{r})d\mathbf{r} \tag{11}$$

is the Fourier transform of the surface elevation. P is the incident wave power captured by the sea surface. The kernel functions of the integral B and M are 2×2 matrices which are mainly dependent on the configuration angles, the polarization, and the complex permittivity of the lower medium. The corresponding details can be found in [34]; here, we safely omit them for the sake of brevity.

For revised CWM, the integral variables $\mathbf{r}$ in (10) should be replaced by $\tilde{\mathbf{r}} = \mathbf{r} + \mathbf{C}_f(\mathbf{r}, t)$; thus, the Jacobian J of the transformation from $\mathbf{r}$ to $\tilde{\mathbf{r}}$ is utilized to accomplish this change of integral variables. Equation (10) should be rewritten as

$$\begin{aligned}\mathbf{S}(\mathbf{k}_i, \mathbf{k}_s; t) = &\frac{2\sqrt{q_0 q_1}}{(q_0+q_1)\sqrt{P}}\int\frac{d\mathbf{r}}{(2\pi)^2}\mathbf{G}(\tilde{\mathbf{r}}, h)\\ &\times\exp\left[-j(\mathbf{k}_1-\mathbf{k}_0)\cdot(\mathbf{r}+\mathbf{C}_f(\mathbf{r}, t))\right.\\ &\left.+j(q_1+q_0)h(\mathbf{r}, t)\right]\\ &\times J(\mathbf{r}, t)\Bigg(B(\mathbf{k}_1, \mathbf{k}_0) - \frac{j}{4}\int M(\mathbf{k}_1, \mathbf{k}_0; \boldsymbol{\xi})\mathbf{H}(\boldsymbol{\xi}, t)\\ &\times\exp(j\boldsymbol{\xi}\cdot\tilde{\mathbf{r}})d\boldsymbol{\xi}\Bigg)\end{aligned} \tag{12}$$

where $J(\mathbf{r}, t) = J_{xx}J_{yy} - J_{xy}J_{yx}$, with individual terms $J_{xx} = 1 + \partial C_{fx}(\mathbf{r}, t)/\partial x$, $J_{yy} = 1 + \partial C_{fy}(\mathbf{r}, t)/\partial y$, $J_{xy} = \partial C_{fx}(\mathbf{r}, t)/\partial y = J_{yx}$, and $\mathbf{C}_f = (C_{fx}, C_{fy})$. The symbol ∂ denotes the calculation of corresponding partial derivatives. Thus, the average NRCS can be expressed as

$$\sigma_{\text{SSA-II}} = 4\pi q_0 q_1\left\langle\left|\mathbf{S}(\mathbf{k}_i, \mathbf{k}_s; t)\right|^2\right\rangle \tag{13}$$

where the angle brackets denote the ensemble average.

Compared with NRCS, the Doppler spectrum of the sea backscattered echoes is a more refined tool to detect the subtle changes in the fluid motion. Furthermore, the hydrodynamic nonlinearities have a dramatic impact on the Doppler spectrum. Thus, the expression of the Doppler spectrum based on the periodogram method [10] is given by

$$S_{\text{Dop}}(f) = \left\langle\frac{1}{T}\left|\int_0^T\mathbf{S}(\mathbf{k}_i, \mathbf{k}_s; t)\exp(-j2\pi f t)dt\right|^2\right\rangle. \tag{14}$$

Like in (13), the angle brackets also denote the ensemble average over much surface realizations. In the following spectra analysis, each Doppler spectrum is evaluated over 120 samples

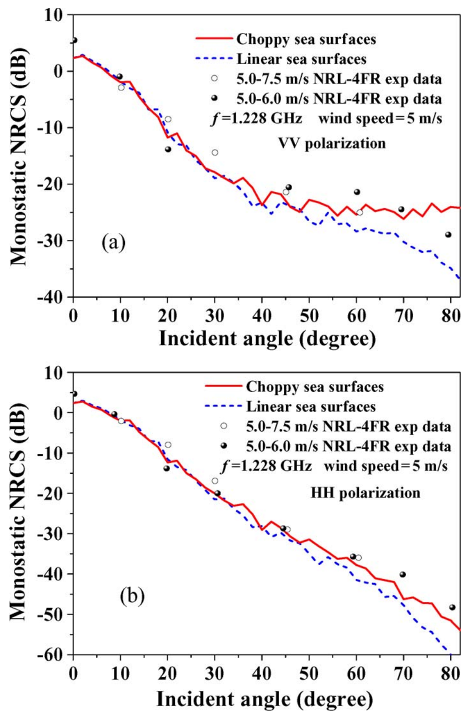

Fig. 5. Monostatic NRCS versus incident angles for choppy surfaces and linear surfaces of infinite-depth seas. The wind speed is 5 m/s. (a) VV polarization. (b) HH polarization.

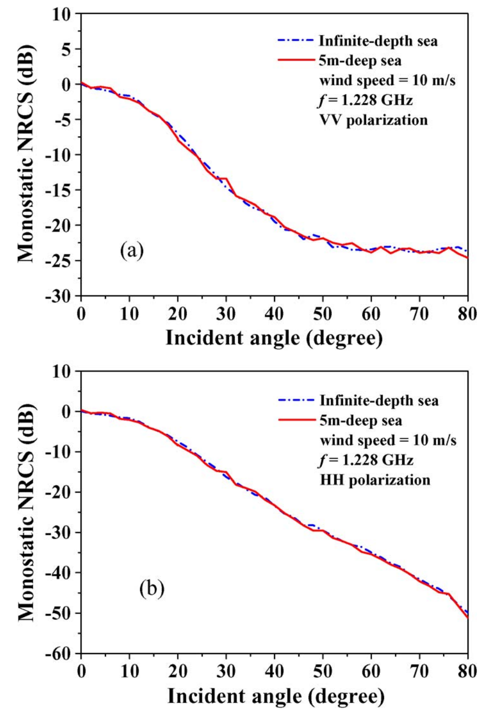

Fig. 6. Comparison of the monostatic NRCS versus incident angles for infinite-depth sea and 5-m-deep sea. The wind speed is 10 m/s. (a) VV polarization. (b) HH polarization.

of the surface realizations involving time-varying sea surfaces with 256 time steps.

IV. Numerical Results and Analysis

It is instructive to compare the monostatic NRCS for the nonlinear hydrodynamic choppy sea surfaces and that for the linear sea surfaces with the experimental measured data. In Fig. 5, the experimental data from the airborne four-frequency radar system of the Naval Research Laboratory [36] for L-band (1.228 GHz) are chosen as a benchmark. Thus, the water depth is set to be infinite. The wind speed is 5 m/s in upwind direction, the size of the sea surface is $L_x = L_y = 128\lambda$, in which λ denotes the incident microwave wavelength, and the surface sample interval is set as $\lambda/8$. The taper wave beam waist is chosen to be $L_x/6$, and the final NRCS is averaged over 40 surface realizations.

It is evident that, in small-incident-angle region, the NRCSs for the choppy surfaces and the linear sea surfaces are nearly the same for both HH and VV polarizations, while for larger angles, it is evident that the results for CWM are larger than that for linear surfaces; this can be explained by the reason that the nonlinear hydrodynamic CWM takes the wave–wave interactions into account. Meanwhile, it is not difficult to see that the results for choppy sea surfaces are more consistent with the experimental data. Thus, the conclusion can be drawn that the validity of the nonlinear hydrodynamic CWM is obtained for infinite-depth sea.

Fig. 6 shows the comparison of the monostatic NRCS for infinite-depth choppy sea surfaces and 5-m-deep choppy sea surfaces. The simulation parameters are the same as those in Fig. 5 except that the wind speed is 10 m/s. It can be seen that the discrepancy of NRCS between these two kinds of surfaces is not great for most of the incident angles, which prompts us to investigate the differences of the Doppler characteristics between these two kinds of surfaces.

Fig. 7 shows the normalized Doppler spectra of the linear surfaces and the nonlinear choppy surfaces of infinite-depth seas. The surface area and corresponding sample interval are the same as those in the aforementioned NRCS calculation. The wind speed is 5 m/s, the incident wave frequency is 1.228 GHz, and the incident angles are fixed at 35° and 70°, respectively. The corresponding Bragg frequencies $f_{\mathrm{Bragg}} = \sqrt{g \sin\theta_i/(\pi\lambda)}$ are noted in the plots by the vertical black solid lines. First, as the incident angle increases, it can be seen that the spectral peaks move closer to the corresponding Bragg frequencies for both linear and nonlinear surfaces. It attributes to the fact that the Bragg scattering component accounts for a larger proportion when the incident angle increases. From 35° to 70°, the Doppler spectra of signals backscattered from linear surfaces become narrower than those from the choppy surfaces. This is due to the fact that the nonlinear-wave components propagate faster than the linear-wave components. Second, for linear surfaces, the spectra for both HH and VV polarizations are centered near the Bragg frequency, while in the case of choppy surfaces, the spectrum for HH polarization is centered at much higher frequency than that for VV polarization; moreover, both of them are farther away from the Bragg frequency. These are attributed to the fact that the CWM corrects the horizontal component of particle velocities by adding a displacement related to the surface elevation to the horizontal position of the particles. It is known to all that these velocities remarkably affect the Doppler spectrum; thus, the shape of the Doppler spectrum is impacted by the modulation of Bragg waves by longer waves. These conclusions are also supported by those found in [37] and [38].

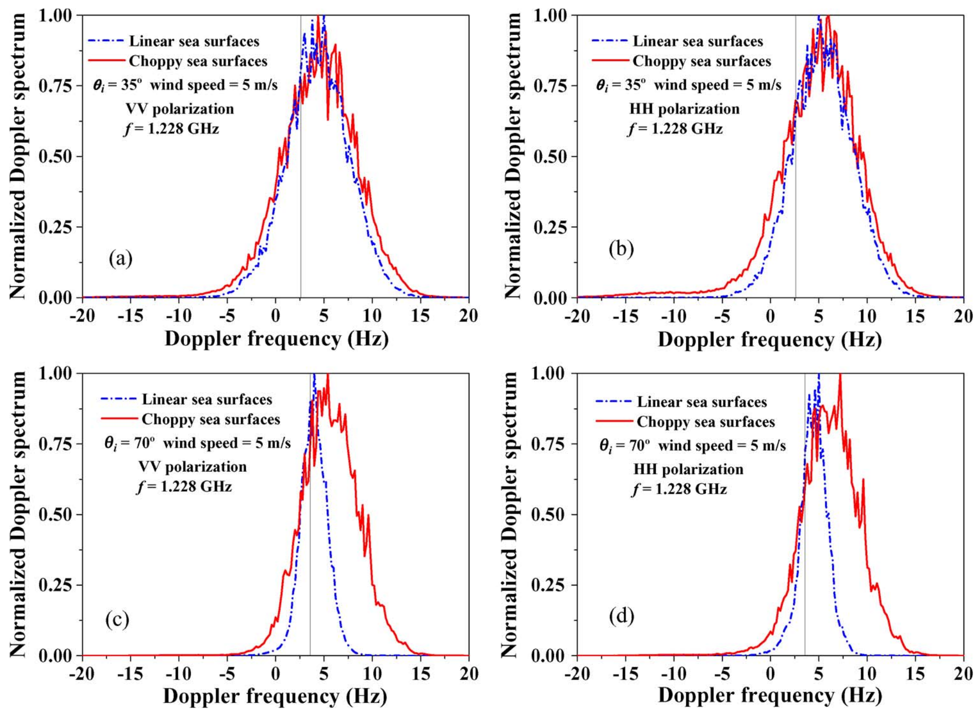

Fig. 7. Comparison of the average normalized Doppler spectra of backscattered echoes from surfaces of infinite-depth linear seas and nonlinear choppy seas at different incident angles. The wind speed is 5 m/s.

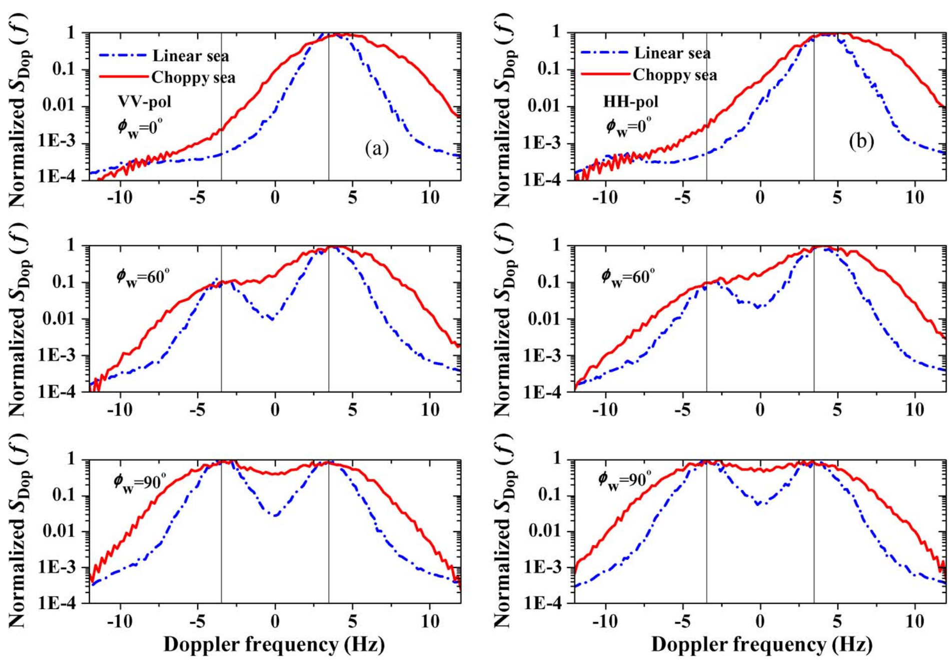

Fig. 8. Average normalized Doppler spectra of backscattered echoes from surfaces of infinite-depth linear seas and nonlinear choppy seas at radar frequency of 1.228 GHz for different wind directions. The incident angle is 70°, and the wind speed is 3 m/s. (a) VV polarization. (b) HH polarization.

To investigate the corresponding characteristics of Doppler spectra for other wind directions aside from upwind, we have performed related simulations to illustrate the influence of the wind direction to the Doppler spectra features in Fig. 8. ϕ_w is designated as the angle between the radar looking direction and the upwind direction. The incident angle is set as 70°, the incident frequency is also 1.228 GHz, and the wind speed is 3 m/s. Three wind directions of $\phi_w = 0^\circ$, 60°, and 90° are presented for comparison. As ϕ_w changes from 0° to 90°, the negative peak appears more and more prominent for both types of sea surface and finally comparable with the positive peak; moreover, compared with linear surfaces, the Doppler spectral widths for nonlinear choppy surfaces are much greater for both polarizations and all three wind directions.

After investigating the Doppler spectrum for deep-sea surfaces, now, we focus on the study of its finite-depth sea counterpart. In [20] and [21], based on the HF radar experiment measured data and Weber and Barrick theory in [39],

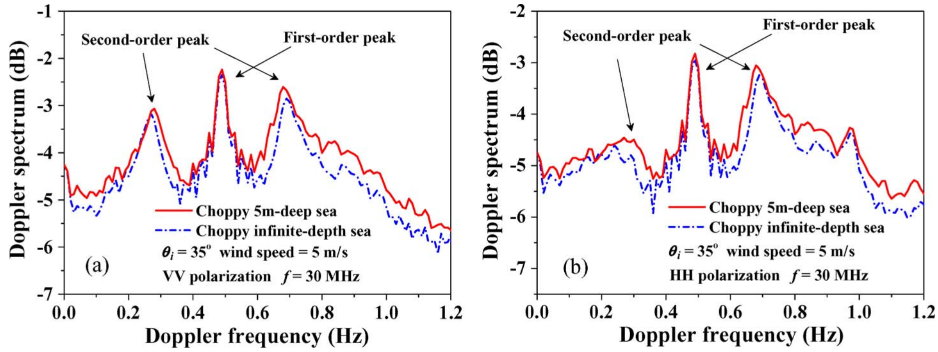

Fig. 9. Comparison of the Doppler spectra for infinite-depth sea and 5-m-finite-depth sea for HF band (30 MHz). The wind speed is 5 m/s, and the incident angle is 35°. (a) VV polarization. (b) HH polarization.

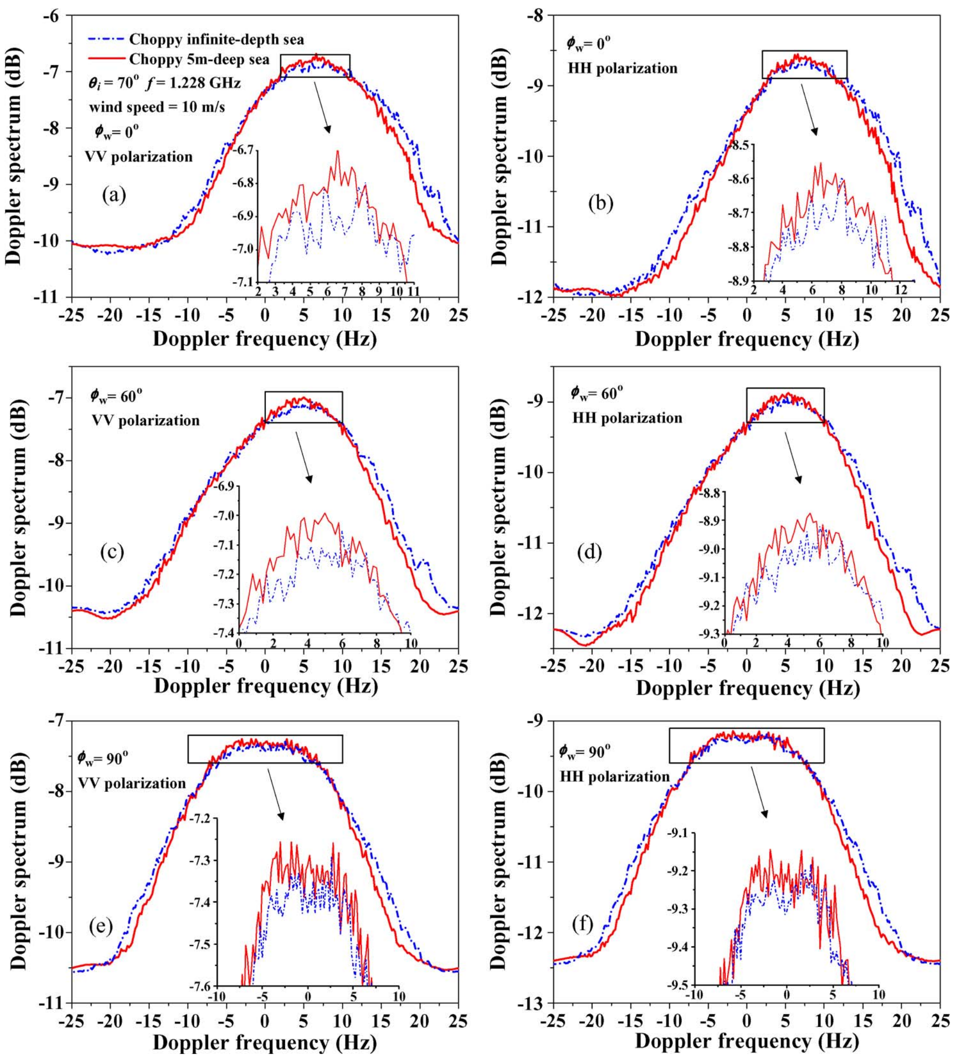

Fig. 10. Comparison of the Doppler spectra for infinite-depth sea and 5-m-finite-depth sea for different wind directions. The wind speed is 10 m/s, the incident angle is 70°, and the radar frequency is 1.228 GHz.

some characteristics of the Doppler spectrum for echoes from shallow-water waves have been observed and verified, which could serve as qualitative arguments to validate our model. Thus, Fig. 9 shows the comparison of the Doppler spectra for backscattered echoes from infinite-depth sea and 5-m-finite-depth sea in the similar HF band circumstance. The incident angles are set as 35°, and the radar frequency is 30 MHz. The wind speed is 5 m/s. It can be found that, when the water depth decreases, the second-order peaks of the Doppler spectrum rise and the amplitude of the second-order spectrum also increases, even if the first-order peaks are nearly at the same level, which are similar to the corresponding features presented in [20] and [21]. Although the origin of this phenomenon has not yet been understood explicitly, it probably implies that strong nonlinear effects are inherent in the finite-depth water wave field.

TABLE I
RUNTIME INVOLVED OF EACH PROCESSOR FOR DOPPLER SIMULATION IN FIG. 10 ON ONE INTEL CORE CPU (2.67 GHz AND 3.21 GB) COMPUTER

Wind direction	Infinite-depth sea		5m-deep sea	
	A single time step(Δt)	All the samples ($\Delta t\times 256\times 120$)	A single time step(Δt)	All the samples ($\Delta t\times 256\times 120$)
$\phi_w = 0^\circ$	4.112s	126330.984s	4.134s	126984.186s
$\phi_w = 60^\circ$	4.118s	126505.452s	4.138s	126969.093s
$\phi_w = 90^\circ$	4.231s	129932.532s	4.285s	131620.537s

Fig. 10 shows the comparison of the Doppler spectra for infinite-depth sea and 5-m-finite-depth sea for different wind directions at L-band (the incident frequency is 1.228 GHz). The incident angle is 70°, and the wind speed is 10 m/s. First, when the wind direction changes from 0° to 90°, it can be seen that the peaks at negative frequency gradually grow in the spectra for both types of surfaces and polarizations. Second, it is not difficult to find that the discrepancy of Doppler spectra attributed to infinite-depth effect is less pronounced when the wind direction changes from upwind direction to crosswind. This observation is similar as in Fig. 8. Finally, it is also noticeable that the spectral amplitudes for finite-depth sea surfaces are much higher than those for infinite-depth surfaces in the frequency range just around the Doppler peak frequency. It is probably a significant sign that the nonlinear-wave–wave interactions are strengthened as the water depth decreases. As waves propagate into finite-depth water from the deep water, the depth effect will work after the waves "touch" the bottom. Due to shoaling, the nonlinear interactions between waves become stronger. The features of the Doppler spectra shown in Figs. 9 and 10 consist of the corresponding simulations verified by experimental measurements in finite-depth sea in [21] and [22] in the qualitative sense. Moreover, from the runtime involved for the Doppler spectra simulation that is shown in Table I, it is indicated that simulations for finite-depth sea surface consume a little more time than those for infinite-depth sea surface, and it is also the same situation when the wind direction changes from upwind to crosswind.

V. CONCLUSION

This paper has investigated the characteristics of the microwave backscattering from the 2-D time-evolving nonlinear surfaces of finite-depth seas using SSA-II in connection with the CWM. A comparative study has been presented to highlight the features of both the NRCS and the Doppler spectra arising from nonlinear hydrodynamic effects and shoaling effects. In infinite-depth sea circumstance, the comparison of the monostatic NRCS for the linear sea model and nonlinear CWM with the experimental measured data shows that the nonlinear CWM has better performance. When both are based on the same nonlinear CWM, the discrepancy between the infinite-depth sea and finite-depth sea for monostatic NRCS is not great. On the other hand, the characteristics of the Doppler spectra for nonlinear choppy sea surfaces are distinct from their counterpart of linear sea surfaces probably due to the nonlinear-wave-wave interactions, which shows that nonlinear hydrodynamics should be given adequate consideration in the Doppler spectra analysis. Furthermore, from the Doppler spectra analysis for nonlinear finite-depth sea in different wind directions, it is demonstrated that the discrepancy of Doppler spectra attributed to infinite-depth effect is less pronounced when the wind direction changes from upwind direction to crosswind. When the water depth decreases, it is also observed that the Doppler spectra have higher second-order peaks and increased spectral amplitudes in the frequency range just around the Doppler peak frequency, which reiterates the importance of the role that the nonlinear hydrodynamics played in the interpretation of backscattering from finite-depth seas. The analysis presented in this paper will help to better investigate the backscattering from the surfaces of finite-depth nearshore seas from the qualitative point of view.

ACKNOWLEDGMENT

The authors would like to thank Dr. A. G. Voronovich for the helpful discussions and the anonymous reviewers for providing invaluable and constructive comments and suggestions.

REFERENCES

[1] K. S. Chen, A. K. Fung, and D. E. Weissman, "A backscattering model for ocean surface," *IEEE Trans. Geosci. Remote Sens.*, vol. 30, no. 4, pp. 811–817, Jul. 1992.

[2] J. T. Johnson, R. T. Shin, J. A. Kong, L. Tsang, and K. Pak, "A numerical study of the composite surface model for ocean backscattering," *IEEE Trans. Geosci. Remote Sens.*, vol. 36, no. 1, pp. 72–83, Jan. 1998.

[3] V. U. Zavorotny and A. G. Voronovich, "Two-scale model and ocean radar Doppler spectra at moderate- and low-grazing angles," *IEEE Trans. Antennas Propag.*, vol. 46, no. 1, pp. 84–92, Jan. 1998.

[4] R. Romeiser and D. R. Thompson, "Numerical study on the along-track interferometric radar imaging mechanism of oceanic surface currents," *IEEE Trans. Geosci. Remote Sens.*, vol. 38, no. 1, pp. 446–458, Jan. 2000.

[5] D. Nie and M. Zhang, "Bistatic scattering analysis for two-dimensional rough sea surfaces using an angular composite model," *Int. J. Remote Sens.*, vol. 32, no. 24, pp. 9661–9672, Dec. 2011.

[6] M. Zhang, H. Chen, and H.-C. Yin, "Facet-based investigation on EM scattering from electrically large sea surface with two-scale profiles: Theoretical model," *IEEE Trans. Geosci. Remote Sens.*, vol. 49, no. 6, pp. 1967–1975, Jun. 2011.

[7] C. L. Rino, T. L. Crystal, A. K. Koide, H. D. Ngo, and H. Guthart, "Numerical simulation of backscattering from linear and nonlinear ocean surface realizations," *Radio Sci.*, vol. 26, no. 1, pp. 51–71, Jan./Feb. 1991.

[8] D. B. Creamer, F. Henyey, R. Schult, and J. Wright, "Improved linear representation of sea surface waves," *J. Fluid Mech.*, vol. 205, pp. 135–161, 1989.

[9] J. V. Toporkov and G. S. Brown, "Numerical simulations of scattering from time-varying, randomly rough surfaces," *IEEE Trans. Geosci. Remote Sens.*, vol. 38, no. 4, pp. 1616–1625, Jul. 2000.

[10] J. V. Toporkov and G. S. Brown, "Numerical study of the extended Kirchhoff approach and the lowest order small slope approximation for scattering from ocean-like surfaces: Doppler analysis," *IEEE Trans. Antennas Propag.*, vol. 50, no. 4, pp. 417–425, Apr. 2002.

[11] B. West, K. A. Brueckner, R. S. Janda, D. M. Milder, and R. L. Milton, "A new numerical method for surface hydrodynamics," *J. Geophys. Res.*, vol. 92, no. C11, pp. 11 803–11 824, Oct. 1987.

[12] J. T. Johnson, J. V. Toporkov, and G. S. Brown, "A numerical study of backscattering from time-evolving sea surfaces: Comparison of hydrodynamic models," *IEEE Trans. Geosci. Remote Sens.*, vol. 39, no. 11, pp. 2411–2420, Nov. 2001.

[13] A. R. Hayslip, J. T. Johnson, and G. R. Baker, "Further numerical studies of backscattering from time-evolving nonlinear sea surfaces," *IEEE Trans. Geosci. Remote Sens.*, vol. 41, no. 10, pp. 2287–2293, Oct. 2003.

[14] G. Soriano, M. Joelson, and M. Saillard, "Doppler spectra from a two-dimensional ocean surface at L-band," *IEEE Trans. Geosci. Remote Sens.*, vol. 44, no. 9, pp. 2430–2437, Sep. 2006.

[15] F. Nouguier, C. A. Guérin, and B. Chapron, "Scattering from nonlinear gravity waves: The 'choppy wave' model," *IEEE Trans. Geosci. Remote Sens.*, vol. 48, no. 12, pp. 4184–4192, Dec. 2010.
[16] F. Nouguier, C. A. Guérin, and B. Chapron, "Choppy wave model for nonlinear gravity waves," *J. Geophys. Res.*, vol. 114, no. C13, pp. C09012-1–C09012-16, Sep. 2009.
[17] F. Nouguier, C. A. Guérin, and G. Soriano, "Analytical techniques for the Doppler signature of sea surfaces in the microwave regime I: Linear surfaces," *IEEE Trans. Geosci. Remote Sens.*, vol. 49, no. 12, pp. 4856–4864, Dec. 2011.
[18] F. Nouguier, C. A. Guérin, and G. Soriano, "Analytical techniques for the Doppler signature of sea surfaces in the microwave regime II: Nonlinear surfaces," *IEEE Trans. Geosci. Remote Sens.*, vol. 49, no. 12, pp. 4920–4927, Dec. 2011.
[19] E. M. Bitner, "Non-linear effects of the statistical model of shallow-water wind waves," *Appl. Ocean Res.*, vol. 2, no. 2, pp. 63–73, Apr. 1980.
[20] D. E. Barrick and B. J. Lipa, "The second-order shallow-water hydrodynamic coupling coefficient in interpretation of HF radar sea echo," *IEEE J. Ocean. Eng.*, vol. OE-11, no. 2, pp. 310–315, Apr. 1986.
[21] B. J. Lipa and D. E. Barrick, "Extraction of sea state from HF radar sea echo: Mathematical theory and modeling," *Radio Sci.*, vol. 21, no. 1, pp. 81–100, 1986.
[22] G. J. Holden and L. R. Wyatt, "Extraction of sea state in shallow water using HF radar," *Proc. Inst. Elect. Eng. F—Radar Signal Process.*, vol. 139, no. 2, pp. 175–181, Apr. 1992.
[23] K. Herterich and K. Hasselmann, "A similarity relation fro the nonlinear energy transfer in a finite-depth gravity-wave spectrum," *J. Fluid Mech.*, vol. 97, no. 1, pp. 215–224, 1980.
[24] C. Bourlier, "Azimuthal harmonic coefficients of the microwave backscattering from a non-Gaussian ocean surface with the first-order SSA model," *IEEE Trans. Geosci. Remote Sens.*, vol. 42, no. 11, pp. 2600–2611, Nov. 2004.
[25] G. Berginc, "Small-slope approximation method: A further study of vector wave scattering from two-dimensional surfaces and comparison with experimental data," *Prog. Electromagn. Res.*, vol. 37, pp. 251–287, 2002.
[26] S. A. Kitaigordskii, V. P. Krasitskii, and M. M. Zaslavskii, "On Phillips's theory of equilibrium range in the spectra of wind-generated waves," *J. Phys. Oceanogr.*, vol. 5, no. 3, pp. 410–420, Jul. 1975.
[27] E. B. Thornton, "Rederivation of the saturation range in the frequency spectrum of wind-generated gravity waves," *J. Phys. Oceanogr.*, vol. 7, no. 1, pp. 137–140, Jan. 1977.
[28] E. Bouws, H. Günther, W. Rosenthal, and C. L. Vincent, "Similarity of the wind wave spectrum in finite depth water 1. Spectral form," *J. Geophys. Res.*, vol. 90, no. C1, pp. 975–986, Jan. 1985.
[29] K. Hasselmann, T. P. Barnett, E. Bouws, H. Carlson, D. E. Cartwright, K. Enke, J. A. Ewing, H. Gienapp, D. E. Hasselmann, P. Kruseman, A. Meerburg, P. Müller, D. J. Olbers, K. Richter, W. Sell, and H. Walden, "Measurements of wind-wave growth and swell decay during the Joint North Sea Wave Project (JONSWAP)," *Dtsch. Hydrogr. Z. Suppl.*, vol. 12, no. A8, pp. 1–95, 1973.
[30] S. Fouques, H. E. Krogstad, and D. Myrhaug, "A second order Lagrangian model for irregular ocean waves," *J. Offshore Mech. Arct. Eng.*, vol. 128, no. 3, pp. 174–183, Aug. 2006.
[31] S. Aberg and G. Lindgren, "Height distribution of stochastic Lagrange ocean waves," *Probab. Eng. Mech.*, vol. 23, no. 4, pp. 359–363, Oct. 2008.
[32] G. Lindgren and S. Aberg, "First order stochastic Lagrange model for asymmetric ocean waves," *J. Offshore Mech. Arct. Eng.*, vol. 131, no. 3, pp. 031602-1–031602-8, Aug. 2009.
[33] M. Miche, "Mouvements ondulatoires de la mer en profondeur constante ou décroissante. forme limite de la houle lors de son d'eferlement. application aux digues marines," *Ann. Ponts Chaussées*, vol. 114, pp. 25–78, 1944.
[34] L. Tsang, J. A. Kong, and K. H. Ding, *Scattering of Electromagnetic Waves*. New York: Wiley, 2001, pp. 270–271.
[35] A. G. Voronovich and V. U. Zavorotny, "Theoretical model for scattering of radar signals in Ku- and C-bands from a rough sea surface with breaking waves," *Waves Random Media*, vol. 11, no. 3, pp. 247–269, 2001.
[36] F. Arikan and N. Vural, "Simulation of sea clutter at various frequency bands," *J. Electromagn. Waves Appl.*, vol. 19, no. 4, pp. 529–542, 2005.
[37] X. F. Li and X. J. Xu, "Scattering and Doppler spectral analysis for two-dimensional linear and nonlinear sea surfaces," *IEEE Trans. Geosci. Remote Sens.*, vol. 49, no. 2, pp. 603–611, Feb. 2011.
[38] F. Forget, M. Saillard, and P. Broche, "Observations of the sea surface by coherent L band radar at low grazing angles in a nearshore environment," *J. Geophys. Res.*, vol. 111, no. C9, pp. C09015-1–C09015-14, 2006.
[39] B. L. Weber and D. E. Barrick, "On the nonlinear theory for gravity waves on the ocean's surface. Part I: Derivations," *J. Phys. Oceanogr.*, vol. 7, no. 1, pp. 3–10, Jan. 1977.

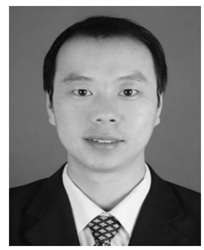

Ding Nie was born in Xinjiang, China, in 1985. He received the B.S. degree in electronic information science and technology from Xidian University, Xi'an, China, in 2007, where he is currently working toward the Ph.D. degree in radio physics in the School of Science.

His research interests include computational electromagnetics and theoretical modeling on electromagnetic scattering rough (sea) surface.

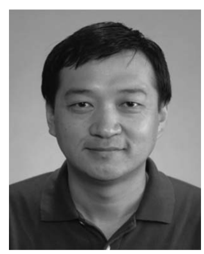

Min Zhang received the B.Sc. degree in physics from Shaanxi Normal University, Xi'an, China, in 1990, the M.Sc. degree in radio physics from Xidian University, Xi'an, in 1998, and the Ph.D. degree in astrometry and celestial mechanics from Shaanxi Astronomical Observatory, Chinese Academy of Sciences, Xi'an, in 2001.

From 2001 to 2003, he was a Postdoctoral Research Fellow in electromagnetic fields and microwave techniques with Xidian University, where he is currently a Full Professor with the School of Science. From May 2003 to October 2004, he was a Research Fellow with the Department of Electrical and Computer Engineering, National University of Singapore, Singapore, Singapore. His current research interests include electromagnetic model design, integral equation techniques, and fast hybrid algorithms for electromagnetic scattering, radiation, and wave propagation.

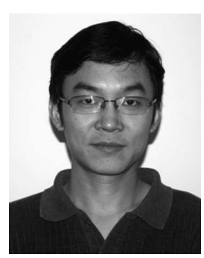

Chao Wang received the B.S. and M.S. degrees from the Northwestern Polytechnical University, Xi'an, China, in 2001 and 2004, respectively, and the Ph.D. degree from the Communication University of China, Beijing, China, in 2009.

After graduation with the M.S. degree, he joined the Science and Technology on Electromagnetic Scattering Laboratory, Beijing. Two years later, he became a Section Chief of the electromagnetic (EM) modeling research group, and he was the principal author of the Radar Target Signature Prediction System which is a suit of EM modeling and simulation software based on high-frequency method and method of moment. He is currently organizing the research group to develop the next generation EM simulation software which integrates EM methods and radar imaging method to simulate the radar echoes and radar images of targets with environment.

Hong-Cheng Yin received the B.S. degree from the Northwest Telecommunication Engineering Institute, Xi'an, China, in 1986, the M.S. degree from the Beijing Institute of Environmental Features, Beijing, China, in 1989, and the Ph.D. degree from the Southeast University, Nanjing, China, in 1993.

From September 1995 to August 2001, he was a Senior Engineer with The Chinese People's Liberation Army (PLA) Air Force Radar Research Institute. Since August 2001, he has been a Researcher with the Science and Technology on Electromagnetic Scattering Laboratory, Beijing. He has coauthored three books and published more than 100 papers in technical journals and conferences. His current research interests include numerical methods in electromagnetic fields, electromagnetic scattering, inverse scattering and propagation, etc.

Dr. Yin is a Fellow of the Chinese Institute of Electronics.